8-2015

Optical anisotropy of porous polymer film with inverse slanted nanocolumnar structure revealed via generalized spectroscopic ellipsometry

Dan Liang
University of Nebraska-Lincoln, dan.liang@huskers.unl.edu

Derek Sekora
University of Nebraska-Lincoln, s-dsekora1@unl.edu

Charles Rice
University of Nebraska-Lincoln, s-crice6@unl.edu

Eva Schubert
University of Nebraska-Lincoln, efranke3@unl.edu

Mathias Schubert
University of Nebraska-Lincoln, mschubert4@unl.edu

Optical anisotropy of porous polymer film with inverse slanted nanocolumnar structure revealed via generalized spectroscopic ellipsometry

Dan Liang,[a] Derek Sekora, Charles Rice, Eva Schubert, and Mathias Schubert
Department of Electrical and Computer Engineering and Center for Nanohybrid Functional Materials, University of Nebraska-Lincoln, Lincoln, Nebraska 68588-0511, USA

(Received 11 June 2015; accepted 11 August 2015; published online 21 August 2015)

We use generalized spectroscopic ellipsometry to characterize the biaxial optical properties of porous polymer and slanted nanocolumnar template thin films. The porous polymer with inverse columnar structure was prepared via infiltrating polymer into the voids of the slanted nanocolumnar film and selectively removing the column material (cobalt). The anisotropic Bruggeman effective medium approximation was employed to analyze the ellipsometry data of the porous polymer film and nanocolumnar template. The classification and structure of optical anisotropy are found to be identical for both samples. The interchangeable optical behaviors between two complementary structures are attributed to the equivalency in their anisotropic polarizabilities. © *2015 AIP Publishing LLC*. [http://dx.doi.org/10.1063/1.4929367]

Porosity provides a significant opportunity for scientists to modify polymeric thin film properties including surface area, morphology, light transmission, etc.[1] In particular, it has been a research focus to tailor the optical properties by introducing pores with variable sizes and shapes to the solid films, because such tunable optical properties allow for the applications of porous polymer films in many areas, such as optical sensing and antireflection coatings.[2–5] Inclusion of nanopores with anisotropic shapes (e.g., ellipsoid and column) in isotropic media leads to anisotropic optical behaviors of porous films.[6] Determination of the anisotropic optical properties, such as anisotropy classification (e.g., tetragonal, monoclinic systems) and structure (sequence of magnitude of principal optical constants, for example, $n_a > n_b > n_c$, with n_a, n_b, and n_c being the refractive indices along each major polarizability axis **a**, **b**, and **c**), becomes crucial to improving the fabrication and design for porous polymer films with desired optical performances.[2–5] Typically, isotropic optical properties are considered in standard ellipsometry analysis on porous polymer films only.[7–11] Recently, generalized spectroscopic ellipsometry (GSE) has been demonstrated to be an excellent method to investigate the form-induced optical anisotropy of porous slanted columnar thin films (SCTFs) prepared via glancing angle deposition (GLAD).[12–17] For instance, GSE has been used to determine the orthorhombic or monoclinic optical properties for SCTFs, including the internal angles between major axes and principal biaxial optical constants.[12,14,18,19] Since GSE is an indirect characterization method, physical models are required to analyze the Mueller matrix data measured on SCTFs. Previously, the anisotropic Bruggeman effective medium approximation (AB-EMA) has been employed to model the GSE data of porous SCTFs to obtain the film thickness, columnar slanting angle, and classes and structures of optical anisotropy.[12,19–21] The AB-EMA is particularly useful for determining the constituent volume fractions of porous SCTFs.[22,23] Therefore, GSE analysis with the AB-EMA provides access to evaluate both structural and optical properties of porous polymer films with inverse columnar structure.

In this work, we utilize GSE to investigate the anisotropic optical properties of porous poly(-methyl methacrylate) thin film with inverse SCTF structure (PMMA iSCTF). The PMMA iSCTF was prepared via infiltration of PMMA into cobalt (Co) SCTF and etch on SCTF templates (Fig. 1(a)). The Mueller matrix element data measured by GSE on PMMA iSCTF and Co SCTF are analyzed by the AB-EMA to determine the structural and biaxial optical properties. From the GSE data analysis, it is revealed that PMMA iSCTF and SCTF can be interchanged without changing the classification and structure of optical anisotropy. Their equivalent optical anisotropy could be due to the similar anisotropic dipole distribution along the nanocolumns or nanopores.

GSE adapts the 4×4 Mueller matrix descriptive system to characterize the optical responses of anisotropic stratified materials.[17] In GSE, the Mueller matrix corresponds to the optical response of the sample and the matrix elements M_{ij} are measured. The AB-EMA model can be used to describe the anisotropic dielectric response of a composite material by assuming highly oriented ellipsoidal inclusions aligned in an isotropic host medium when the inclusion size is small compared with the wavelength of the light. In the AB-EMA, the effective dielectric function along the three major axes **a**, **b**, and **c** for a composite with n components is expressed as[17]

$$\sum_{i=1}^{n} f_i \frac{\varepsilon_i - \varepsilon_{\mathrm{eff},j}}{\varepsilon_{\mathrm{eff},j} + L_j(\varepsilon_i - \varepsilon_{\mathrm{eff},j})} = 0, \; j = \mathrm{a,b,c}, \tag{1}$$

where ε_i and f_i denote the bulk dielectric function and volume fraction of the ith component of the composite, respectively, $\varepsilon_{\mathrm{eff},j}$ represents the effective dielectric function along the three major axes **a**, **b**, and **c**. L_a, L_b, and L_c are the three depolarization factors along **a**, **b**, and **c**, respectively, with $L_\mathrm{a} + L_\mathrm{b} + L_\mathrm{c} = 1$.[17,24] The three factors are dependent on the inclusion shape defined by the dimension ratios between the axes.[17,24] With the AB-EMA, the dielectric response of

[a]Electronic mail: dan.liang@huskers.unl.edu

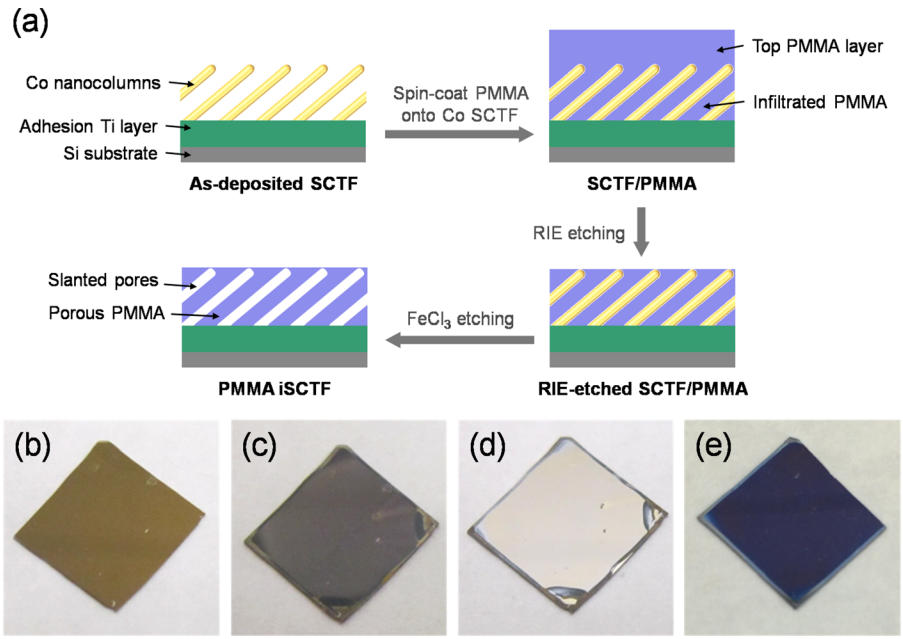

FIG. 1. The scheme in (a) depicts the preparation process for PMMA iSCTF. The photographs of the sample are: (b) the as-deposited Co SCTF; (c) the Co SCTF coated with PMMA after RIE; (d) the PMMA iSCTF after $FeCl_3$ wet etching; and (e) a 90 nm solid PMMA film spin-coated on Si substrate. The size of the sample is approximately 1 cm × 1 cm.

SCTFs is found to be biaxial with the **c** axis along the long axis of the nanocolumns as shown in Fig. 2(a).[20–22] In this work, it is assumed in the AB-EMA for PMMA iSCTF that slanted nanocolumnar pores are highly aligned in the PMMA matrix with the **c** axis along the long axis of the nanopores as shown in Fig. 2(b). Note that the AB-EMA is valid because the pore diameter is far below the wavelength range of interest here.

Figs. 1(a)–1(e) depict the preparation process for the PMMA iSCTF. Via our GLAD system, the Co SCTF was first deposited onto a silicon (Si) substrate coated with a 30 nm adhesion titanium (Ti) layer. The details of the deposition are described elsewhere.[15,17] Second, 2.5 wt. % of PMMA (Sigma-Aldrich) dissolved in toluene was spin-coated onto the as-deposited SCTF at a speed of 3000 rpm for 60 s, and the PMMA-coated SCTF was baked at 165 °C for 1 h. Third, reactive ion etching (RIE) was utilized to remove the extra PMMA layer on the top of Co SCTF. Finally, the Co SCTF was selectively removed by submersion into an aqueous iron chloride ($FeCl_3$) solution (1M) and rinsed with deionized water. The obtained iSCTF sample was then dried in a convection oven at 60 °C for 2 h. Figs.

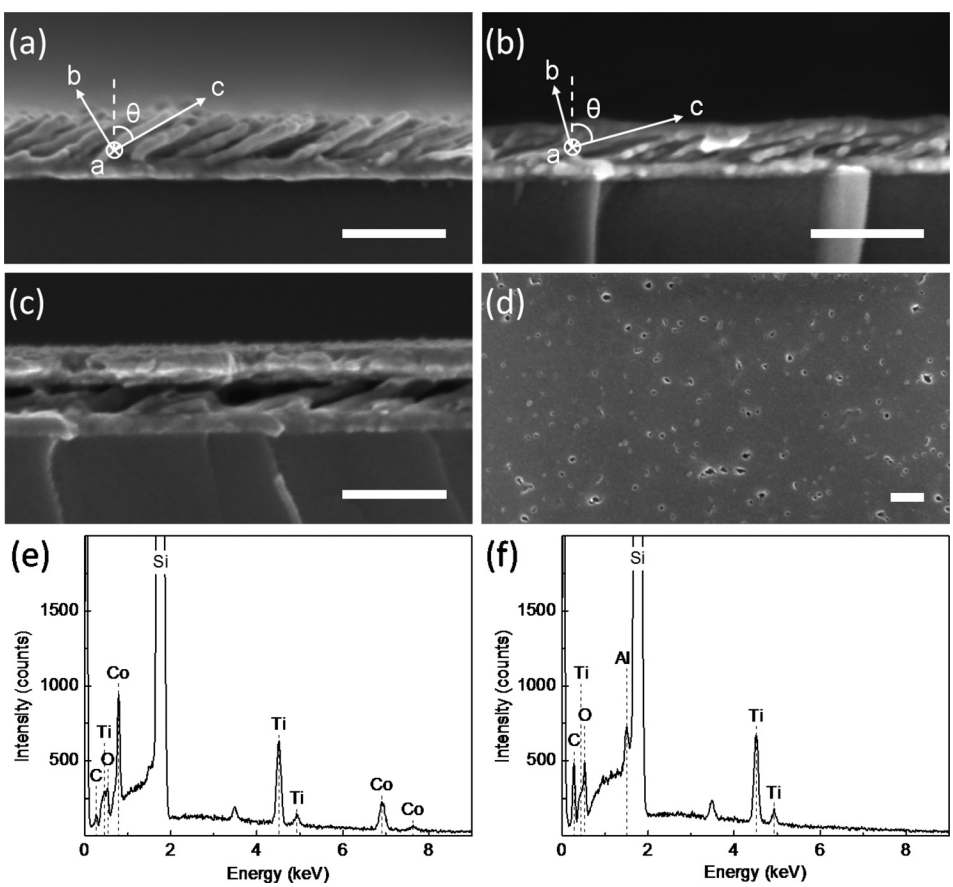

FIG. 2. The cross-section SEM images of (a) the as-deposited Co SCTF, (b) PMMA iSCTF coated with 5 nm of Al_2O_3, (c) Al_2O_3-coated PMMA iSCTF with 45 nm top Ti layer and top-view SEM image of (d) PMMA iSCTF coated with 8 nm Ti. Scale bar: 200 nm. The overlaid schemes in (a) and (b) depict the orthorhombic system with the **c** axis along the orientation of the slanted nanocolumns or nanopores and **a** axis parallel to the film surface. The slanting angle θ represents the angle between **c** and the substrate surface normal (dashed line). EDX spectra of (e) the as-deposited Co SCTF and (f) PMMA iSCTF coated with 5 nm of Al_2O_3.

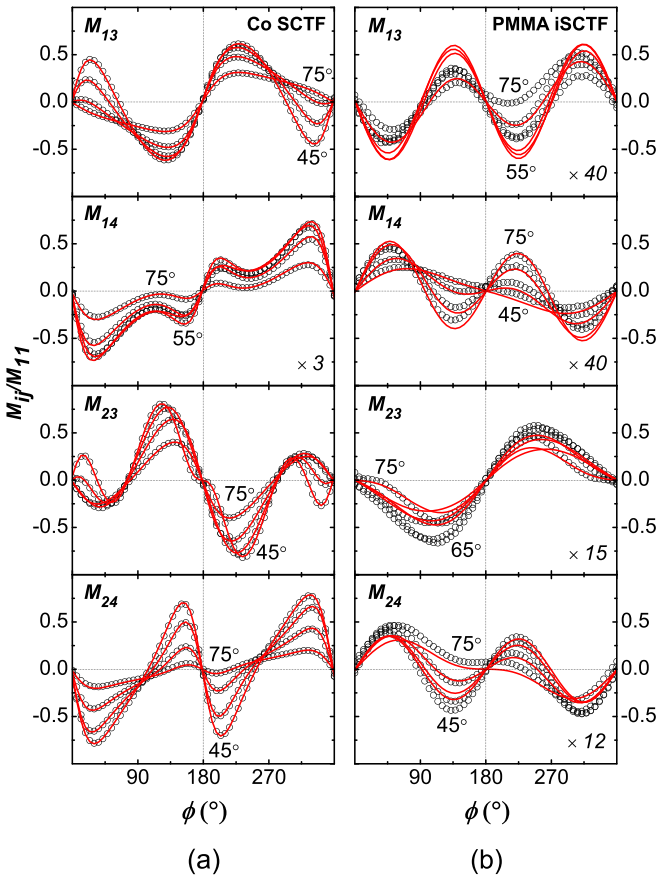

FIG. 3. Experimental (open circles) and best-model calculated (solid lines) off-diagonal-block Mueller matrix elements M_{ij} normalized to M_{11} versus sample azimuth ϕ and angle of incidence $\Phi_a = 45°$, 55°, 65°, 75° at $\lambda = 485$ nm. Columns (a) and (b) show data for the as-deposited Co SCTF and PMMA iSCTF, respectively. Data are scaled up by the multiplication factor given in the lower right corner of individual graphs.

1(b)–1(d) show photographs of the sample at different preparation steps. The PMMA iSCTF in Fig. 1(d) shows good transparency such that the Si substrate is visible and differs from the color appearance of a 90 nm solid nonporous PMMA film on Si as shown in Fig. 1(e). The GSE data measurements were conducted on the Co SCTF and PMMA iSCTF within the spectral range from 400 nm to 1700 nm using a commercial ellipsometer (M-2000VI, J. A. Woollam Co., Inc.). The angle of incidence Φ_a was varied from 45° to 75° in steps of 10° and at each Φ_a the sample azimuth angle ϕ was rotated from 0° to 360° in steps of 6°. For the SEM (Nova NanoSEM 450, FEI) analysis, Ti (8 nm for top view SEM and 45 nm for cross-section SEM) and aluminum oxide (Al_2O_3; 5 nm) coatings were deposited on the PMMA iSCTF with the GLAD and atomic layer deposition (ALD) systems (Fiji 200, CambridgeNanoTech, Inc.), respectively, to protect the polymer from electron beam damage. Energy dispersive X-ray spectroscopy (EDS) spectra of Co SCTF and PMMA iSCTF coated with Al_2O_3 were measured with an EDS spectrometer (Oxford Instruments) operating at 15 kV.

The cross-section image of PMMA iSCTF in Fig. 2(b) shows the pores with shape of slanted columns within the PMMA matrix, which indicates that the PMMA iSCTF and Co SCTF template are structurally complementary to each other. The slanting angle of the nanopores is evaluated to be 71 ± 3° from Fig. 2(b). From Fig. 2(c), the total thickness for Al_2O_3-coated iSCTF plus the top Ti layer is determined to be 140 ± 4 nm. Subtracting the thicknesses of 5 nm for Al_2O_3 and 45 nm for Ti, we determine the thickness for iSCTF to be approximately 90 nm. Fig. 2(d) shows a top-view SEM of the PMMA iSCTF. Figs. 2(e) and 2(f) show the EDX spectra of the Co SCTF, and PMMA iSCTF coated with Al_2O_3, respectively. Fig. 2(f) shows no signals from Co element (EDX detection limit on transition metals is typically in the order of 0.1 wt. % [Ref. 25]), indicating $FeCl_3$ etching effectively removed the Co slanted columns.

Fig. 3 depicts selected experimentally determined off-diagonal-block Mueller matrix elements M_{ij} normalized to M_{11} for the as-deposited Co SCTF and PMMA iSCTF. Data for Co SCTF resemble those presented previously and are not further discussed here.[14–16] On-diagonal-block elements M_{ij} for iSCTF are omitted further for brevity, while off-diagonal-block elements are discussed below. Although the magnitudes of the off-diagonal-block elements and their variation versus sample azimuth ϕ are substantially decreased for the iSCTF sample, the off-diagonal-block elements indicate optical anisotropy within the iSCTF since these elements are zero for isotropic samples.[15] This optical anisotropy results from the anisotropic pore shape within PMMA. The iSCTF data exhibit a two-fold rotational symmetry versus sample azimuth ϕ similar to Co SCTF. The two pseudoisotropic sample orientations of the iSCTF with $M_{ij} \approx 0$ occur at $\phi \approx 0°$ and $\phi \approx 180°$, equivalent to the Co SCTF where the plane of incidence is parallel to the nanopore or nanocolumn orientation, respectively.[14,15] The similarity in the off-diagonal Mueller matrix data reveals that the PMMA iSCTF resembles Co SCTF template in its anisotropic optical response. This similarity is attributed to the resemblance in structural anisotropy since both samples are composed of slanted columnar inclusions highly oriented in an isotropic medium.

A stratified optical model was utilized to analyze the experimental GSE data. For the Co SCTF, the optical model comprises an isotropic Si substrate, an isotropic adhesion Ti layer (thickness t_a), and an anisotropic (AB-EMA) layer (thickness t_f). The AB-EMA layer accounts for the biaxial dielectric response of the SCTF and includes the bulk optical constants of Co and void ($n = 1$, $k = 0$). The orientation of the major polarizability axes in AB-EMA layer is depicted in Fig. 2(a). In our nomenclature, β denotes the internal angle between **b** and **c**.[26] The Euler angle θ indicates the angle between the **c** axis and the substrate surface normal (slanting angle of the nanocolumns). The bulk optical constants of Co are parameterized using sums of harmonic oscillator functions to maintain Kramers-Kronig consistency and reduce the numbers of unknown parameters. For the PMMA iSCTF, the model consists of a Si substrate, a Ti layer (thickness t_a), and an AB-EMA layer (thickness t_f). The AB-EMA layer accounts for the iSCTF and comprises the bulk optical constants of Co, PMMA, and void. As depicted in Fig. 2(b), θ denotes the slanting angle of the nanopores. The bulk optical constants of Co determined previously in the modeling for Co SCTF and those of PMMA determined by a Cauchy model were kept constant during the modeling for the iSCTF. The biaxial optical response of the iSCTF is considered to be orthorhombic with $\beta = 90°$. In the modeling for both samples, the

TABLE I. The best-model parameters for the as-deposited Co SCTF and PMMA iSCTF. The error bars given in parentheses denote the numerical uncertainty of the last digit (90% confidence interval).

Parameter	Co SCTF	PMMA iSCTF
t_f (nm)	83.07(8)	95.9(1)
θ (deg)	59.68(1)	70.5(7)
f_v (%)	78.96(2)	36.6(2)
f_{Co} (%)	21.04(2)	0.15(1)
f_p (%)	N/A	63.2(2)
t_a (nm)	31.29(8)	34.8(1)
β (deg)	90.03(4)	90(fixed)
L_a	0.4112(4)	0.456(4)
L_b	0.5096(4)	0.320(4)
L_c	0.0792(6)	0.224(3)

experimental and model-calculated data are matched as close as possible by varying the model parameters (best-model). As shown in Fig. 3(a), the best-model calculated data for Co SCTF are in a good agreement with experimental data. In Fig. 3(b), small differences can be seen between the best-model and experimental data for iSCTF; however, the best-model calculation matches the data signatures versus sample azimuth and angle of incidence excellently.

The structural parameters of the samples determined by the best-model analysis of the AB-EMA are shown in Table I. The best-model results represent the averaged physical properties over the measured spot on the samples. The error bars in the table denote the finite uncertainty which is related to the measurement accuracy and best-model calculation process. The best-model results for the Co SCTF show a film thickness (t_f) of 83 nm and slanting angle (θ) of 60° approximately which are highly consistent with the values found via SEM analysis (82 nm and 61°, respectively). θ for the PMMA iSCTF is determined to be 70° which is in good agreement with SEM result showing $\theta \approx 71°$. The thickness of the iSCTF given by best-model is 96 nm which is slightly above the SEM result with $t_f \approx 90$ nm. The best-model results for the iSCTF reveal that the Co volume fraction parameter f_{Co} is decreased significantly from 21.04% to 0.15% which is consistent with the vanished Co EDX signal in Fig. 2(f). The PMMA fraction f_p is the largest with 63.2% indicating PMMA becomes the main constituent in this iSCTF. The void fraction f_v is determined to be 36.6% by the best-model which confirms the porous structure within the film. The parameter t_a values for both samples are consistent with the intended adhesion layer thickness of 30 nm. Compared the depolarization factors of the Co SCTF, it is found that for the iSCTF, L_b decreases and L_c increases while the change in L_a is relatively small, but L_c still shows the lowest value compared with L_a and L_b, indicative of a cylindrical pore shape elongated along the **c** axis. We find that β is approximately 90° for both Co SCTF and iSCTF, and thus both films reveal orthorhombic optical anisotropy along axes **a**, **b**, and **c**.

Fig. 4 depicts the effective optical constants along the three major axes of the as-deposited Co SCTF and PMMA iSCTF which are obtained by the best-model calculation based on the AB-EMA approach. For the Co SCTF, the optical constants along axis **c** show strongest wavelength dependency. For the PMMA iSCTF, the optical constants along each axis reduce substantially due to the removal of Co. k_a, k_b, and k_c are nearly zero in the spectral range investigated, which is indicative of high transparency for iSCTF. The refractive indices of the iSCTF along each axis show a small wavelength dependency similar with that of the solid PMMA film obtained by a Cauchy model. n_a, n_b, and n_c are lower than the refractive indices of the solid PMMA film (between 1.49 and 1.51 approximately), which reflects the porous structure within the iSCTF. The structure for optical anisotropy becomes $n_c > n_a > n_b$ in the entire spectral range, thus **c** remains as the axis of the PMMA iSCTF for which the largest dielectric polarizability occurs. For ease of

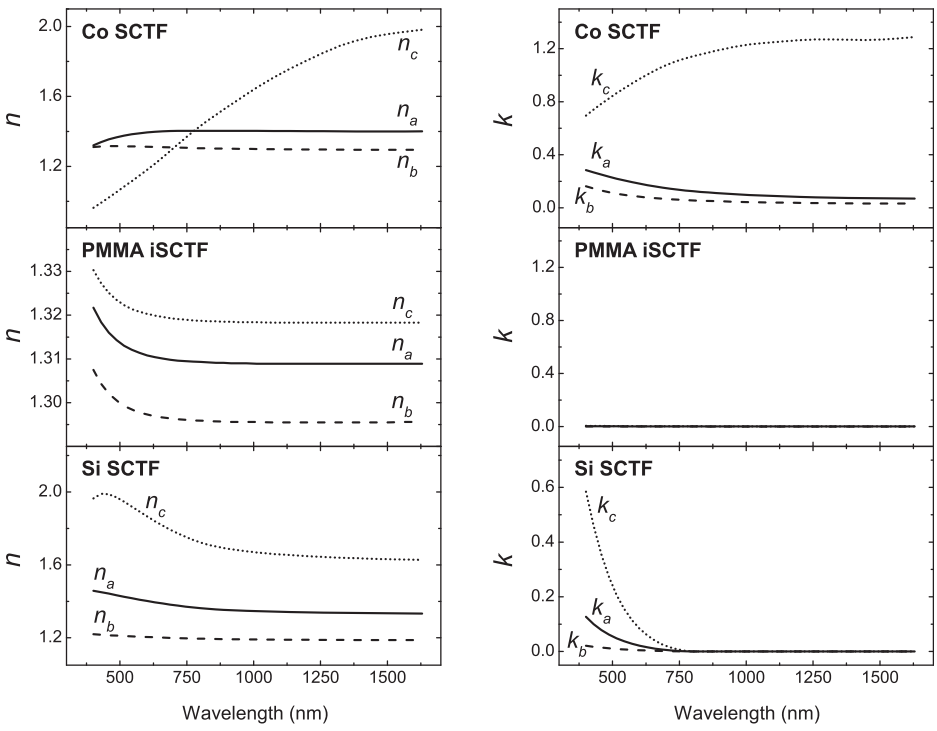

FIG. 4. Effective optical constants, n_j and k_j (j = a, b, c), along the major axes **a** (solid lines), **b** (dashed lines), and **c** (dotted lines) determined by the AB-EMA for the as-deposited Co SCTF, PMMA iSCTF, and Si SCTF.

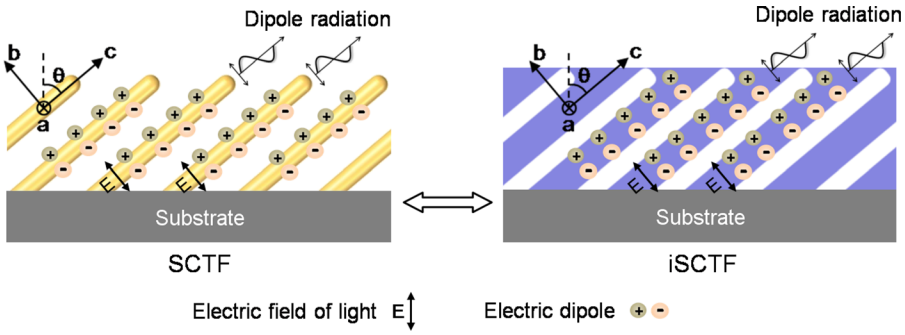

FIG. 5. Diagram of electric dipole distribution for SCTF and iSCTF which results in the anisotropic polarizability.

comparison, the effective refractive indices of Si SCTF ($t_f = 109$ nm, $\beta = 88°$, and $\theta = 62°$) which is nearly lossless in this spectral range are exhibited in Fig. 4.[17] It is noted that $n_c > n_a > n_b$ holds over the entire spectral range for Si SCTF. Therefore, despite different materials producing different absolute values of optical constants, the samples with complementary physical structures possess identical structure for optical anisotropy.

From the best-model results in Table I, it is noted that f_v for PMMA iSCTF is larger than f_{Co} for the as-deposited SCTF. This difference indicates that extra PMMA was removed along with Co nanocolumns during the $FeCl_3$ etching. In addition, L_c for the iSCTF becomes larger than Co SCTF, which reveals that the dimension ratios of **a** and **b** to **c** axis increase for the nanopores. Thus, the pore structure becomes less elongated along **c**. This lateral increase could be explained by the excess PMMA removal during the etching process.

The present work investigates two complementary structures: slanted nanocolumns embedded in void and slanted nanopores embedded in polymer. The equivalency in optical response (identical class and structure of optical anisotropy) can be explained by similarity in anisotropic polarizabilities of the two structures. Fig. 5 illustrates the electric dipole distribution due to the incident light with electric field perpendicular to either nanocolumns or nanopores. The dipole radiation dependent on the polarizability is the source for the optical response of materials.[27] When SCTFs are present, the polarizability along **b** axis results from the dipoles oriented perpendicularly to slanted nanocolumns. When the slanted nanopores replace nanocolumns, the dipoles oriented perpendicularly to slanted nanopores become the source for the polarizability along **b**. Notwithstanding different structures, the PMMA iSCTF and SCTFs show similar anisotropic dipole distribution along the long axis, which results in similar polarizability along **b**. The same explanation applies to the polarizabilities along **a** and **c** axes.

In conclusion, the structural and optical properties of the PMMA iSCTF and SCTF template are obtained via the AB-EMA modeling of GSE data. The structural parameters such as film thickness and slanting angle show good agreement with SEM analysis. The anisotropic optical properties for both samples are determined to be orthorhombic. The PMMA iSCTF possesses the same order for the effective refractive indices with SCTFs. The elongated dipole distribution for the two complementary structures causes the similarity in their polarizabilities, therefore leading to the identical class and structure for optical anisotropy.

The authors would like to acknowledge the financial support from the National Science Foundation (EPS-1004094 and MRSEC DMR-0820521), the University of Nebraska-Lincoln, and the J. A. Woollam Foundation.

[1]D. Wu, F. Xu, B. Sun, R. Fu, H. He, and K. Matyjaszewski, Chem. Rev. **112**, 3959 (2012).
[2]J. Huang, C. A. Tao, Q. An, W. Zhang, Y. Wu, X. Li, D. Shen, and G. Li, Chem. Commun. **46**, 967 (2010).
[3]X. Li, J. Gao, L. Xue, and Y. Han, Adv. Funct. Mater. **20**, 259 (2010).
[4]M. Ibn-Elhaj and M. Schadt, Nature **410**, 796 (2001).
[5]K. D. Harris, J. C. Sit, and M. J. Brett, IEEE Trans. Nanotechnol. **1**, 122 (2002).
[6]L. A. Golovan, P. K. Kashkarov, and V. Yu. Timoshenko, Crystallogr. Rep. **52**, 672 (2007).
[7]M. S. Silverstein, M. Shach-Caplan, B. J. Bauer, R. C. Hedden, and H. J. Lee, Macromolecules **38**, 4301 (2005).
[8]J. S. Kim, H. C. Kim, B. Lee, and M. Ree, Polymer **46**, 7394 (2005).
[9]T. Oka, K. Ito, M. Muramatsu, T. Ohdaira, R. Suzuki, and Y. Kobayashi, J. Phys. Chem. B **110**, 20172 (2006).
[10]C. Sinturel, M. Vayer, M. Morris, and M. A. Hillmyer, Macromolecules **46**, 5399 (2013).
[11]M. Vayer, T. H. Nguyen, D. Grosso, C. Boissiere, M. A. Hillmyer, and C. Sinturel, Macromolecules **44**, 8892 (2011).
[12]J. Gospodyn and J. C. Sit, Opt. Mater. **29**, 318 (2006).
[13]I. S. Nerbø, S. L. Roy, M. Foldyna, M. Kildemo, and E. Søndergård, J. Appl. Phys. **108**, 014307 (2010).
[14]D. Schmidt, B. Booso, T. Hofmann, E. Schubert, A. Sarangan, and M. Schubert, Appl. Phys. Lett. **94**, 011914 (2009).
[15]D. Schmidt, A. C. Kjerstad, T. Hofmann, R. Skomski, E. Schubert, and M. Schubert, J. Appl. Phys. **105**, 113508 (2009).
[16]D. Schmidt, B. Booso, T. Hofmann, E. Schubert, A. Sarangan, and M. Schubert, Opt. Lett. **34**, 992 (2009).
[17]D. Schmidt and M. Schubert, J. Appl. Phys. **114**, 083510 (2013).
[18]R. A. May, D. W. Flaherty, C. B. Mullins, and K. J. Stevenson, J. Phys. Chem. Lett. **1**, 1264 (2010).
[19]G. Beydaghyan, C. Buzea, Y. Cui, C. Elliott, and K. Robbie, Appl. Phys. Lett. **87**, 153103 (2005).
[20]T. Hofmann, D. Schmidt, A. Boosalis, P. Kühne, R. Skomski, C. M. Herzinger, J. A. Woollam, M. Schubert, and E. Schubert, Appl. Phys. Lett. **99**, 081903 (2011).
[21]D. Schmidt, E. Schubert, and M. Schubert, Appl. Phys. Lett. **100**, 011912 (2012).
[22]T. Kasputis, M. Koenig, D. Schmidt, D. Sekora, K. B. Rodenhausen, K. J. Eichhorn, P. Uhlmann, E. Schubert, A. K. Pannier, M. Schubert, and M. Stamm, J. Phys. Chem. C **117**, 13971 (2013).
[23]D. Liang, D. Schmidt, H. Wang, E. Schubert, and M. Schubert, Appl. Phys. Lett. **103**, 111906 (2013).
[24]T. G. Mackay and A. Lakhtakia, J. Nanophotonics **6**, 069501 (2012).
[25]P. M. Wilson, G. N. Mbah, T. G. Smith, D. Schmidt, R. Y. Lai, T. Hofmann, and A. Sinitskii, J. Mater. Chem. C **2**, 1879–1886 (2014).
[26]D. Schmidt, E. Schubert, and M. Schubert, "Generalized ellipsometry characterization of sculptured thin films made by glancing angle deposition," in *Ellipsometry at the Nanoscale* (Springer, Berlin, 2013), pp. 341–410.
[27]H. Fujiwara, *Spectroscopic Ellipsometry Principles and Applications* (John Wiley & Sons, New York, 2007).